sustainability

MDPI

Article

Sustainable Architecture Creating Arches Using a Bamboo Grid Shell Structure: Numerical Analysis and Design

Faham Tahmasebinia [1,*], Yuanchen Ma [1], Karl Joshua [1], Saleh Mohammad Ebrahimzadeh Sepasgozar [2], Yang Yu [1], Jike Li [1], Samad Sepasgozar [3] and Fernando Alonso Marroquin [1]

[1] School of Civil Engineering, The University of Sydney, Sydney, NSW 2006, Australia; yuma4447@uni.sydney.edu.au (Y.M.); kjos0802@uni.sydney.edu.au (K.J.); yayu3122@uni.sydney.edu.au (Y.Y.); jili7122@uni.sydney.edu.au (J.L.); fernando.alonso@sydney.edu.au (F.A.M.)
[2] Babol Noshirvani University of Technology, Babol 47148, Iran; s.sepasgozar@yahoo.com
[3] Faculty of Built Environment, The University of New South Wales, Sydney, NSW 2052, Australia; sepas@unsw.edu.au
* Correspondence: Faham.tahmasebinia@sydney.edu.au

Abstract: Bamboo is known as a sustainable alternative for green building design, and it has been tied culturally to some regions around the world. However, bamboo's structural strength for different design scenarios needs more investigation before it is widely adopted. Timber and bamboo have similar mechanical properties, but the latter is a repaid, renewable, sustainable, disaster-resilient system and is versatile, which has more advantages for construction purposes. Natural bamboo and its derivatives have been considered as a high-demand green and environmentally responsible alternative construction material, and this interest is increasing globally. Because of the rapid growth rate and large developing area, it is more useable than the limited timber resource. However, natural bamboo has an anisotropic and nonhomogeneous material property, which varies in multiple directions. There is limited engineering data and investigation of bamboo material and its use in and impact on construction. In this study, three different bamboo models were analyzed by Strand7; each of them had different features in structure and in the major construction material. A new model was proposed by improving the three given structures and was maximized in the mechanical capacity. Some design guidelines were proposed based on the analysis and comparison of different bamboo structures. The model will replace natural bamboo with bamboo scrimber, which is an engineered bamboo derivative that has more uniform material properties.

Keywords: sustainable design; green structure; curved elements; bamboo; dynamic load; grid shell; arch

check for updates

Citation: Tahmasebinia, F.; Ma, Y.; Joshua, K.; Sepasgozar, S.M.E.; Yu, Y.; Li, J.; Sepasgozar, S.; Marroquin, F.A. Sustainable Architecture Creating Arches Using a Bamboo Grid Shell Structure: Numerical Analysis and Design. *Sustainability* **2021**, *13*, 2598. https://doi.org/10.3390/su13052598

Academic Editors: Giouli Mihalakakou and Miguel Amado

Received: 29 January 2021
Accepted: 22 February 2021
Published: 1 March 2021

Publisher's Note: MDPI stays neutral with regard to jurisdictional claims in published maps and institutional affiliations.

Copyright: © 2021 by the authors. Licensee MDPI, Basel, Switzerland. This article is an open access article distributed under the terms and conditions of the Creative Commons Attribution (CC BY) license (https://creativecommons.org/licenses/by/4.0/).

1. Introduction

Bamboo is traditionally known as one of the popular materials for vernacular architecture [1,2]. However, recent studies suggest this material to be used for modern architecture [3]. The main purpose of this study was to present alternative design models using a bamboo grid shell structure, which has better mechanical capacity under various load conditions and in both static and dynamic analysis. At the same time, bamboo is known as a relatively environmentally friendly material and is sustainable [4]. Finite element analysis was conducted to analyze the strength and serviceability of natural bamboo and bamboo scrimber using Strand7 [5]. Three structures constructed by natural bamboo and variants in design were analyzed by replacing their construction material with bamboo scrimber. Then, a new structure was proposed based on the comparison and analysis of three given structures, and some design improvements were addressed in a new structure. Three initial models were constructed in AutoCAD and were transferred to Strand7 for finite analysis; the improved, new design was fully constructed using Strand7 alone (See Figure 1).

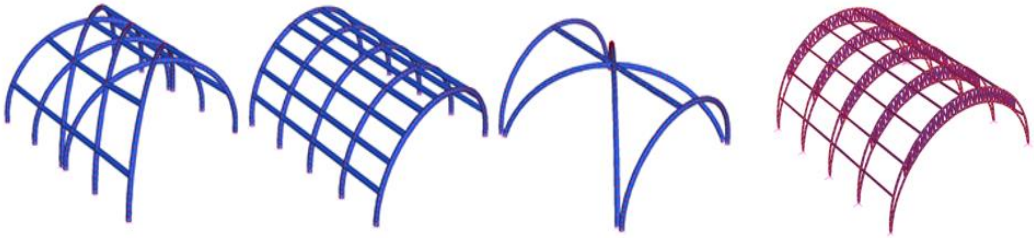


Figure 1. Preliminary model (blue) and improved model (pink).

In this study, the main innovation was to suggest an alternative material and a curved structure design. As a rapidly growing and wild developing material, bamboo has been used for construction purposes for a long time in many tropical areas. It is a similar material to timber but with less weight and greater flexibility. As sustainable construction has been proposed as a green strategy this century, the interest in using bamboo has been increasing. However, natural bamboo not only has a nonhomogeneous and anisotropic property but its size varies from bottom to top. Thus, it is not suitable for modern construction, which requires uniform construction material. Natural bamboo grows straight with a circular hollow section, and there are limited data and investigation about using natural bamboo in a curved shape for constructing a roof. Therefore, bamboo scrimber was chosen alternatively as a better construction material [4,6]. Bamboo scrimber can maintain the material property of bamboo and can be made in any desired shape. Some relevant literature demonstrates bamboo scrimber as a good alternative construction material. Thus, by using bamboo scrimber with the desired member shape, it is easier to design and construct a suitable and stable structure.

Although more attention has been paid to the advantage of using bamboo as a construction material, there is still a lack of investigation conducted regarding its mechanical properties and its guidelines in construction [7–12]. The goal of this study was to propose new ideas about taking the advantages of bamboo and its derivatives and investigating potential improvement for a bamboo structure as a major construction material. With the investigation, the aim was to assist the future study and design of bamboo structures [12–15].

2. Materials and Methods

2.1. The Material Properties

Bamboo scrimber was chosen as the major construction material, although its material property data are limited. The first reason to choose this material is the increasing interest in bamboo as a construction technique, which is due to its being a popular, recyclable, and sustainable material [16–20]. Furthermore, in comparison, bamboo timber is more suitable for construction purposes because it can be made in any desired shape and has a uniform property, whereas natural bamboo is hard to be curved and has a circular hollow section and an anisotropic and nonhomogeneous property. Natural bamboo needs to go through many procedures to become a bamboo scrimber. As bamboo scrimber production technology develops, some procedures have been cut for large scale production; the main process is a composite of truncation and splitting, defibering, drying, dipping, assembly, cold-pressing, and heat-curing or hot-pressing, which is highly material efficient, utilizing approximately 80% of raw inputs [20,21]. Moreover, it maintains the longitudinal direction of the bamboo fibers and utilizes the resin matrix to connect the fiber bundles.

The material properties of bamboo scrimber can be impacted by multiple perspectives, such as the production procedure and the species of bamboo used to produce scrimber. The analysis of bamboo scrimber structure will also be impacted because of the uncertainty of the material properties. The common property range of bamboo scrimber is listed in the table below (Table 1).

Table 1. Bamboo scrimber's mechanical properties.

Property	Value
Elastic modulus (E)	13.5–32.3 GPa
Poisson's ratio	0.26–0.52
Density (p)	720–1300 kg/m^3

Some experiment was implemented to test the ultimate capability of bamboo scrimber because of the effect of the different mechanical conditions. Because of the internal and small fiber structure, bamboo scrimber performs differently when the load acts in a different direction. Normally, when the load acts parallel to the grain, bamboo scrimber can perform well. In contrast, if the loading mechanism acts perpendicular to the grain, bamboo scrimber's capacity will drop significantly. Local failure will happen when the specific stress exceeds the material capacity, and all the local failure stresses of bamboo scrimber under each loading mechanism acting parallel to the grain is shown in the table below (Table 2).

Table 2. Ultimate stresses of bamboo scrimber.

Property	Value
Tension [2]	296.2 MPa
Compression [2]	134.9 MPa
Bending [4]	119 MPa
Shear [4]	15 MPa

If any load mechanism exceeds the given value in the table above, local failures of bamboo scrimber will occur and result in a cracking and fiber separation of bamboo scrimber, which causes global failure. All these values were used to analyze the structure in this study.

2.2. Comparison between Bamboo Scrimber, Natural Bamboo, and Timber

Because of the limited research and investigation, bamboo scrimber has rarely been used for construction purposes. However, bamboo scrimber has many advantages over other timber materials and natural bamboo, such as high dimensional stability. Its mechanical properties are normally influenced by the bamboo species used and by the manufacturing technology. In Table 3, the material properties of multiple engineered timbers and bamboo derivatives are compared. This table shows the advantage and shortcomings of each material and proves that bamboo scrimber has the capability to be used as a construction material.

Table 3. Material properties for structural timber and bamboo comparison.

Material	Density ρ kg/m^3	Compression f_c (Mpa)	Tension f_t (Mpa)	Shear τ (Mpa)	Flexural f_b (Mpa)
Bamboo scrimber	1010	134.9	296.2	15	119
Raw bamboo	666	53	153	16	135
Sitka spruce	383	36	59	9	67
Douglas-fir	520	57	49	11	68

As presented in Table 3, it can be found that bamboo scrimber has a relatively high density compared with other materials. Furthermore, the table also shows that the mechanical properties of bamboo scrimber are better than all other materials, except raw bamboo, which has a better shear and bending capacity. However, these bamboo scrimbers show similar bending and shear capacity to natural bamboo. Overall, bamboo scrimber is more suitable for construction.

Although natural bamboo is cheaper and has relatively better performance than other timber material, it still has some significant shortcomings. The first one is its anisotropic and nonhomogeneous property, which varies along with the whole bamboo, whereas bamboo scrimber has a uniform property, which is easier to be used and analyzed in design. Furthermore, because of the circular shape, the stable connection between natural bamboo is hard to be achieved all the time, which limits the structure design. This is also the main reason to develop bamboo scrimber, which inherits all the advantages of raw bamboo and can be designed in any expected shape. However, as the bamboo derivate, bamboo scrimber also has some similar shortcomings as natural bamboo. The mechanical performance of both heavily depends on the load and fiber direction; when the stress is parallel to the grain, they have better performance. In contrast, when the load is perpendicular to the grain, their mechanical property drops significantly.

Multiple factors can impact the material properties of bamboo scrimber. Its properties are formed heavily and depend on the manufacturing process. Because of the highly compacted structure and low moisture content, it has high density, compression, and tension capacity. It also inherits almost all shear and bending capacity from natural bamboo. The key manufacturing processes that decides bamboo scrimber's material properties are drying, dipping, and pressing. Most of the moisture is extracted during the drying procedure, which controls the moisture content of bamboo scrimber below 10% and improves its Young's modulus and internal bond strength. The dipping process also contributes to the density and bonding performance; the resin is used to dip the dried bamboo fiber, which bonds them together and provides some extra features, such as waterproof capacity. Moreover, the bamboo fired will be pressed under very high pressure; this procedure reduces its Poisson's ratio significantly and could make it in the desired shape.

2.3. Model

2.3.1. Three Initial Designs

The preliminary three designs are provided below. All three designs consisted of curved bamboo elements, which were used for shaping a grid-like spatial structure. The arch members were used in all the design scenarios, including the bracing in design 2 and crossover members in the rest of the design scenarios. In all three scenarios, a layer of a thin glass panel was used as a roof, and the weight of the glass was supported by curve bamboos.

During the modelling process, all the bamboo curved roofs adopted the same geometry properties, as shown in the Figure 2 below. They were initially modelled as 0.0045 m square sections using manufactured bamboo scrimbers, and the mechanical properties are mentioned in the available literature. It enables the possibility of maintaining the consistency in size and properties of the bamboo elements throughout the structure.

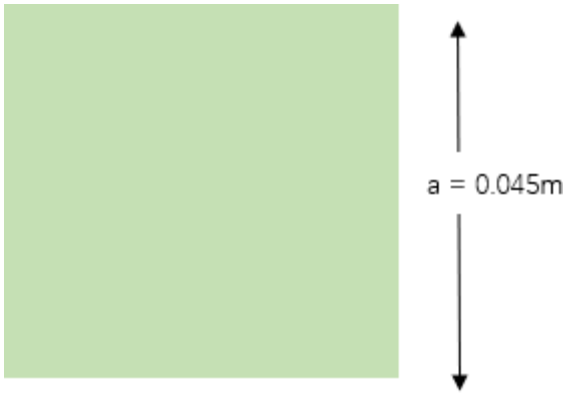


Figure 2. Cross-section of the beam element in the model using a solid square bamboo scrimber with a length of 0.045 m.

The relevant property values assigned in Strand7 for performing numerical analysis are summarized in the table below (Table 4).

Table 4. The presented mechanical properties of the bamboo scrimber.

Property	Value
Elastic modulus (E)	2.29×10^{10} Pa
Poisson's ratio	0.39
Density (p)	1010 kg/m^3
Length (a)	0.045 m

2.3.2. Initial Structure: Design 1

Figure 3 demonstrates the details of the design 1 suggested frame. Design 1 took into account the circular arches that crossover to demonstrate the lateral support of the structure. This crossover can transfer the critical stresses to the adjusting members. This is a novel structural technique to distribute critical stresses.

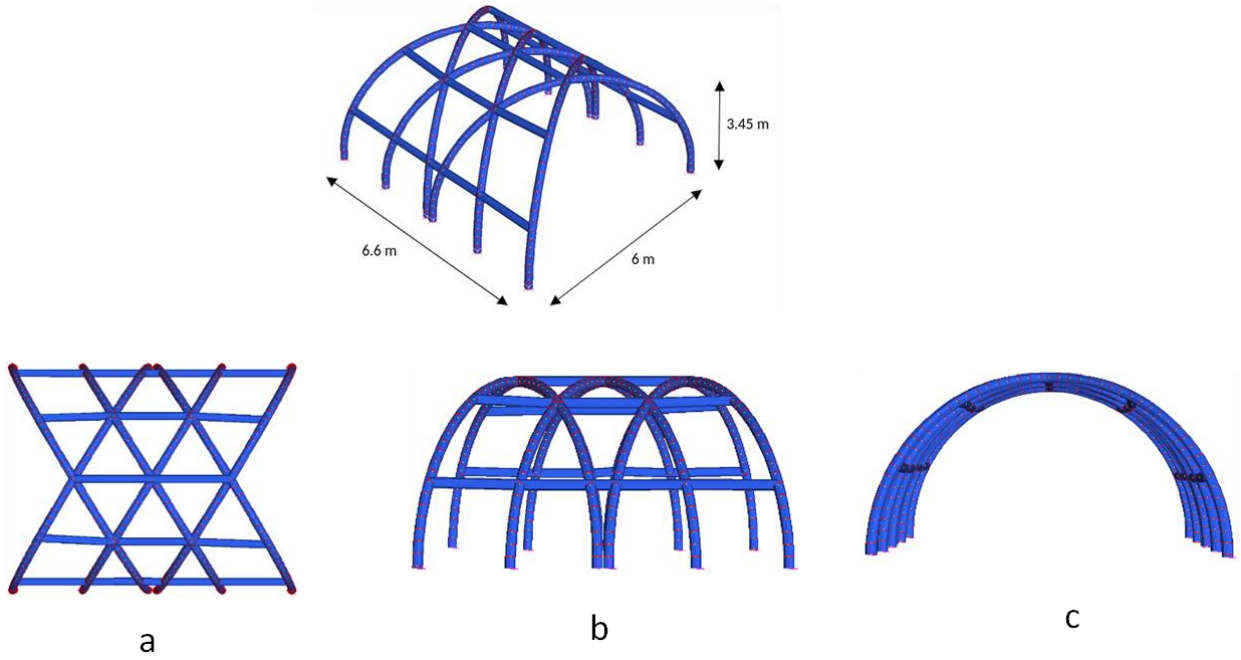


Figure 3. Overview of the design 1 structure: (**a**) plan view, (**b**) side view, and (**c**) front view.

2.3.3. Initial Structure: Design 2

Figure 4 presents the details of the design 2 suggested frame, which covered all aspects of the stability of the structural system. A conventional arch was taken into account in the proposed design, which can follow the design in a typical barrel vault approach. There was no crossover of arches in this design, meaning that the transfer of lateral force is only via the horizontal bamboo members.

2.3.4. Initial Structure: Design 3

Figure 5 presents the details of the design 3 suggested frame in the structural frame system. Design 3 was included a combination of proposed elements, which were presented in designs 1 and 2.

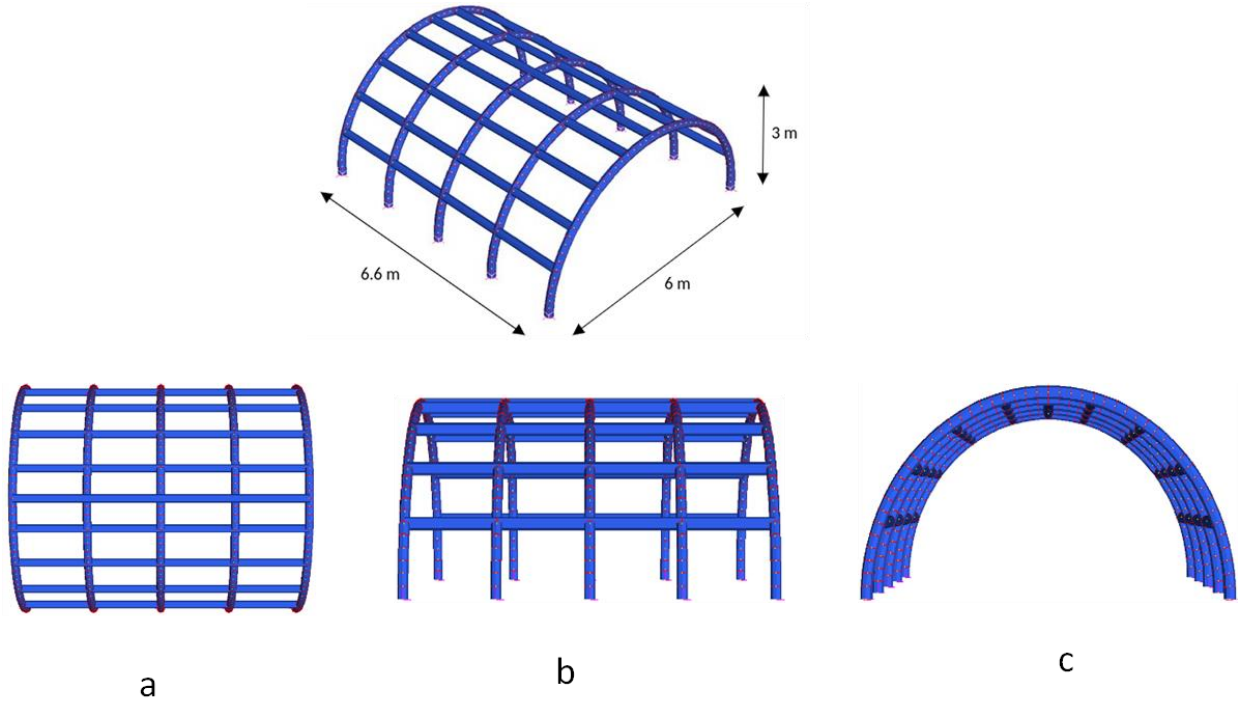


Figure 4. Overview of the design 2 structure: (**a**) plan view, (**b**) side view, and (**c**) front view.

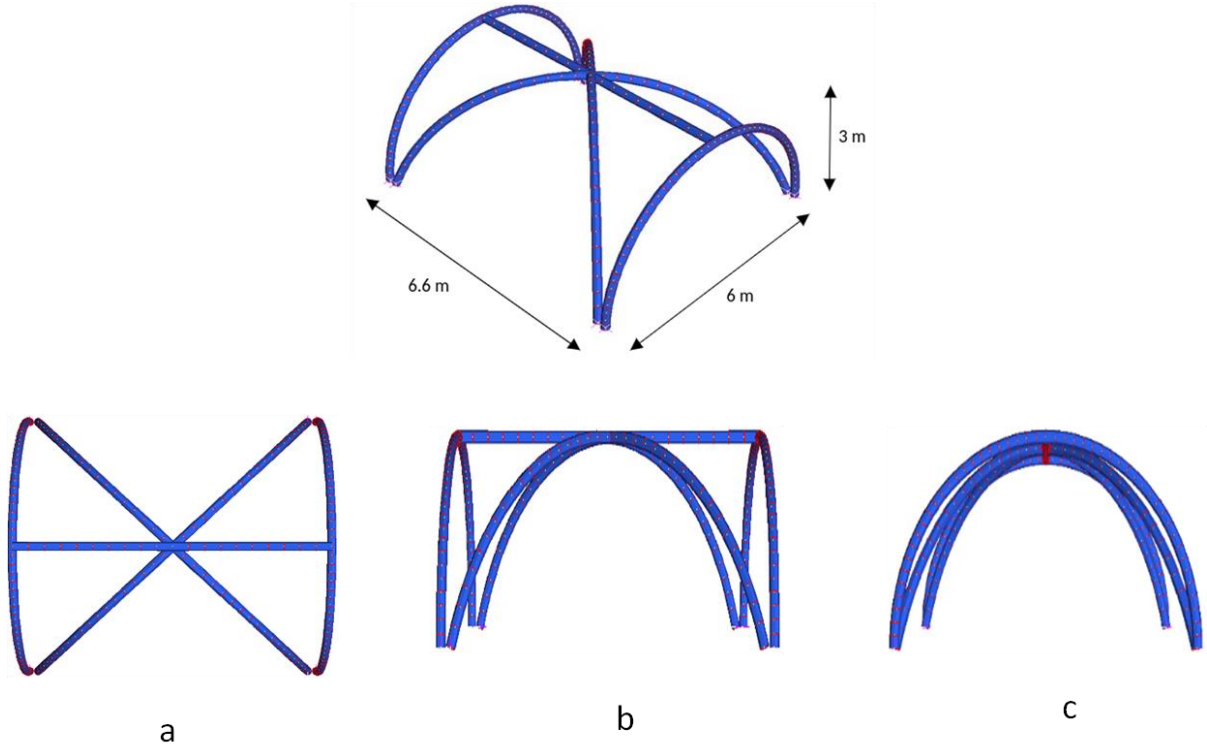


Figure 5. Overview of the design 3 structure: (**a**) plan view, (**b**) side view, and (**c**) front view.

2.3.5. Improved, New Design

Figure 6 demonstrates the details of the new suggested design for the frame system. The new design was based on a typical barrel vault formation, with double arches for each of the arch structures, which aimed to estimate truss structures between the upper and lower arches. The truss system enables the distribution of the loads from the upper arch to

the lower arch and hence eases the loads throughout the structure. It further enhanced the reliability of initial design 2 by adding the lower arch and the truss system. The connections at the base are mentioned in the literature review.

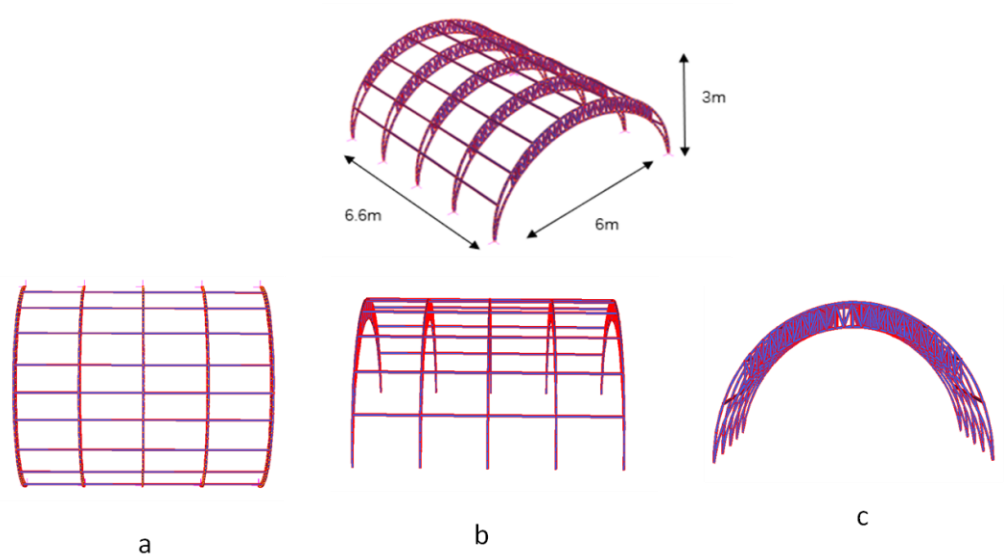


Figure 6. Overview of the proposed new design: (**a**) plan view, (**b**) side view, and (**c**) front view.

The load distribution of this new design is similar to the proposed initial structure design 2. Therefore, for the sake of simplicity, the static load conditions (the dead load, live load, and static wind load and their corresponding load combination cases) were the same as described in initial structure design 2.

2.3.6. Loads

Four different loading conditions or assumptions were considered in this study for performing load analysis as listed below:

- 470 kPa for the weight of roofing material, which is glass roofing.
- 9.9 kN/m^3 for the weight of the selected bamboo scrimber.
- 0.25 kPa for the proposed live load on the floor.
- The Australian standard was considered for calculation of wind pressures; an Australian metropolitan area was chosen as the proposed location of the structure. The standard suggestion of a 500-year recurrence interval was adopted. More specifically, a combination of AS1170.2 [22–24] and Eurocode 1 [25,26] was used since the structure was a curved shape.

The dead weight of bamboo scrimber was automatically calculated in Strand7. It was achieved by simply choosing the gravity load under the dead load case and summing the node reaction forces at the global vertical direction (in our cases, it was the global y-direction in Strand7). The applied live load of 0.25 kPa was typical of the roofing as per AS1170.0 and assumed that there was no access to pedestrians. Within the scope of the analysis in this report, this was a satisfactory approximation. G presents the deal load, Q presents live load, and W is the applied wind load.

The proposed new design used the same load cases as mentioned above, and this is reasonable as the glass was installed on the top arches such that the lower arches would not withstand the dead load directly from the glass. With the advent of the truss system, the live load was also applied to the top arches only and then transferred to the lower arches, and so was the static wind load.

Figure 7 shows the load conditions for a selected arch structure as part of design 1, and the tributary width was constructed in a conservative manner considering the largest value in that region. However, the upper level of the arch gave zero tributary width.

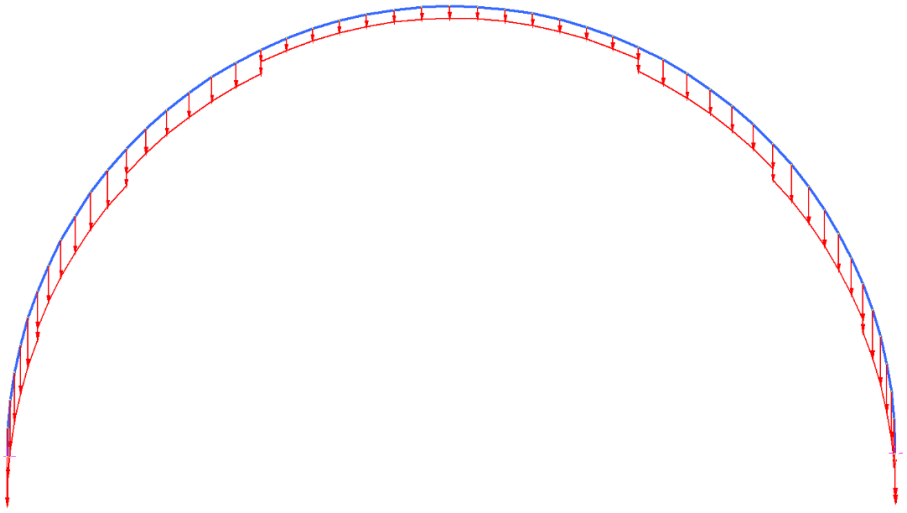


Figure 7. General load conditions for a typical arch structure in initial design 1.

The Australian standard of AS1170 [22] was used for combination alternatives, including both serviceability and ultimate limits. The minimum requirement for considering the section capacity in each scenario of design modeling, the worst-case limiting state, was computed and considered. The worst-case states were identified by computing each of the five load combinations listed below:

- Ultimate limiting state:
  - 1.35 G
  - 1.2 G + 1.5 Q
  - 1.2 G + W + Q
- Serviceability limiting state:
  - G + Q
  - G + 0.7 Q + W

In order to make the design models comparable, circular arches were considered for modeling purposes, and the result is shown in Figure 8. The workflow was considered based on the downward proposed loads, which were from the top into the rigid connections at the base of the structure via the arches.



Figure 8. Load path of the three initial designs.

As for the proposed new design, because of the presence of the lower arches and the truss system, the load distribution followed a similar mode as mentioned above but was converted to multiple paths, which further demonstrates that the new design can help ease the load in a distributed manner (Figure 9).

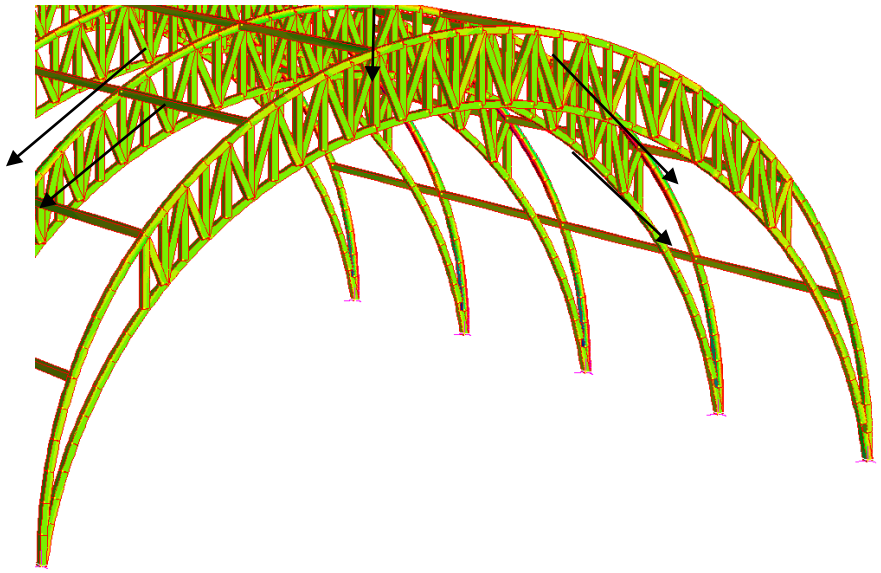


Figure 9. Load path of the new proposed design. The arches behind the front one followed the same distribution pattern. Because of the size of the picture, it does not appear on the figure.

2.3.7. Numerical Analysis

The three initial designs were modelled in AutoCAD and then imported into Strand7 for numerical analysis as beam elements. The curved elements were subdivided into small pieces and connected by sufficient nodes with small and regular intervals to achieve a more accurate result. Distinct from the three initial designs, the new proposed design was fully established in Strand7. The coordinates of the nodes for forming the arch structures were determined based on developed functions. The functions of the upper arch and the lower arch were determined using the expression of circular standard equations.

The selected material properties of bamboo scrimber were assigned in Strand7. A summary of the ultimate strength for the manufactured bamboo scrimber is indicated in Table 5.

Table 5. Material capacity of bamboo scrimber.

Property	Ultimate Strength Capacity (MPa)
Tensile stress	296.2
Compressive stress	134.9
Shear stress	15.0
Bending stress	119.0
Fiber stress	54.3

As for the boundary conditions, the base nodes were fully fixed in all directions. It prevented the movement of base nodes in any direction and the rotation of the structure at the foundations, which followed the same base conditions in reality. For the static load and load combination cases of all the four models as described in the loads section of this study, it used the linear static solver to perform various analysis. Apart from these, it used the natural frequency solver to determine sufficient modes of the house and then performed the spectral response solver to obtain the performance of the models under dynamic wind load. This was because the spectral response analysis requires a mode superposition

procedure where the natural modes are essential for determining their responses under dynamic loads.

3. Results

3.1. Buckling Evaluation in the Curved Beams

In this section, the results of buckling assessments for curved members are discussed (Figure 10). In order to consider the safest design, the worst-case state was considered as the largest radius arches for this assessment. Equation (1) was used for assessing the buckling of uniformly compressed curved arches [27].

$$w = A\ sin\ k\theta + B\ cos\ k\theta \tag{1}$$

$$q_{cr} = \frac{EI}{R^3}\left(\frac{\pi^2}{\alpha^2} - 1\right) \tag{2}$$

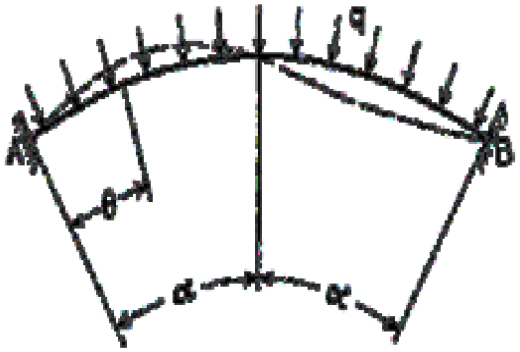


Figure 10. Buckling of a uniformly compressed circular arch.

In the case of the selected designs, the values to be used in the calculation above are given in Table 6, which were calculated from the properties and dimensions of the designs.

Table 6. Values required for critical buckling load per curved member. The top arch of the new design had the same values as the values in design 2. Hence, the new design column in the table only demonstrated the values of the lower arch.

Values	Design 1	Design 2	Design 3	New Design (Bottom)
E	2.29×10^{10} Pa	2.29×10^{10} Pa	2.29×10^{10} Pa	2.29×10^{10} Pa
I	3.42×10^{-7} m^4	3.42×10^{-7} m^4	3.42×10^{-7} m^4	3.42×10^{-7} m^4
R	3.43 m	3.00 m	4.71 m	2.5 m
α	$\frac{\pi}{2}$	$\frac{\pi}{2}$	$\frac{\pi}{2.6202}$	$\frac{\pi}{2}$
Critical buckling Load (q_{cr})	0.58 kN/m	0.87 kN/m	0.44 kN/m	1.5 kN/m

As can be seen from Table 6, the critical variable was the largest curvature R. Based on Equation 2, one can see that R is inversely proportional to the critical buckling load. This means that a shorter radius can lead to a bigger buckling capacity. This is also proved by the values in Table 6; the lower arch of the new design had the smallest R but the largest q_{cr}. Moreover, from previous studies, with a similar size scale for one certain curved bamboo member, natural bamboo would have a larger value of I, which would result in larger values of q_{cr}.

However, since these calculations were indicated by respecting Timoshenko's theory of elastic stability [27], the computed values were overestimated, which means the buckling capacity of each arch should be smaller in reality. This is because the uneven distribution of stress was not considered when performing the approximation of elasticity. Furthermore, the restraints from crossed arches in models 1 and 3 were also not considered nor were the restraints from the glass connection points. Hence, the results are not fully accurate.

It can be concluded that the critical values of buckling load for bamboo scrimber are relatively smaller than natural bamboo, demonstrating that manufactured bamboo scrimber could have a greater risk of undergoing buckling than natural bamboo.

3.2. Static Load Analysis of Three Initial Designs

For each model, two serviceability limiting state (SLS) and three ultimate limiting state (ULS) load cases according to AS1170.0 [22], as well as the load case with wind load only, are presented below. The critical cases (shown in Figures 11–15) for the load cases were selected as the maximum value of the displacement and stresses, which were considered independently. For all the cases, the results shown are from 45 mm width square cross-section bamboo scrimber, based on the numerical analysis from Strand7.

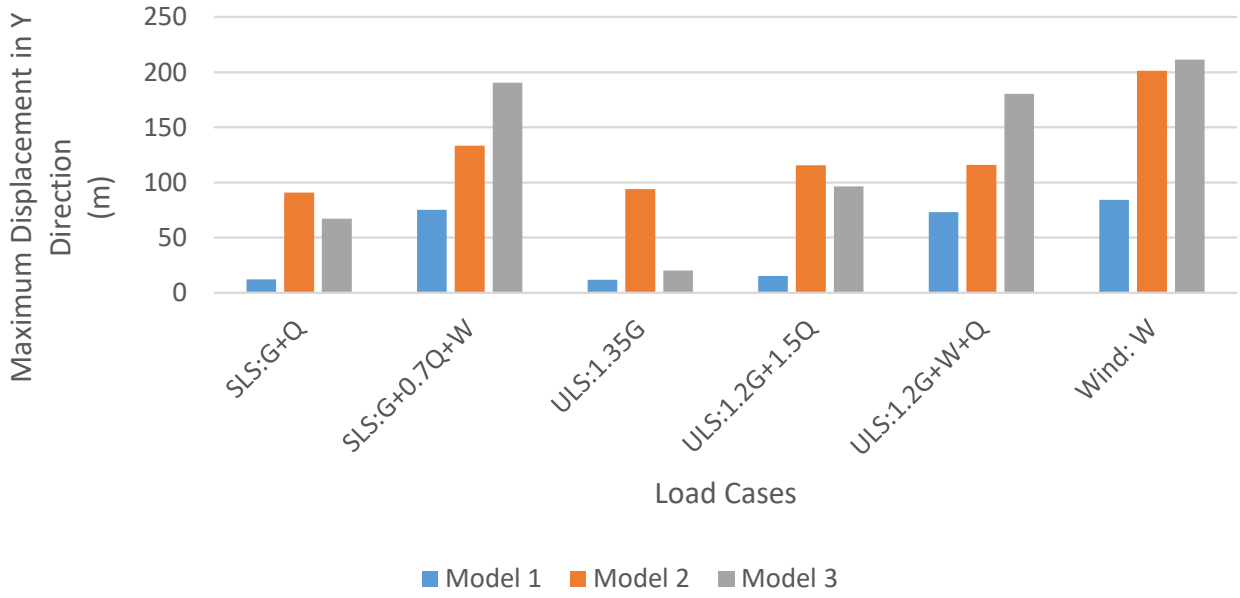


Figure 11. Maximum displacement results for varying load cases and models.

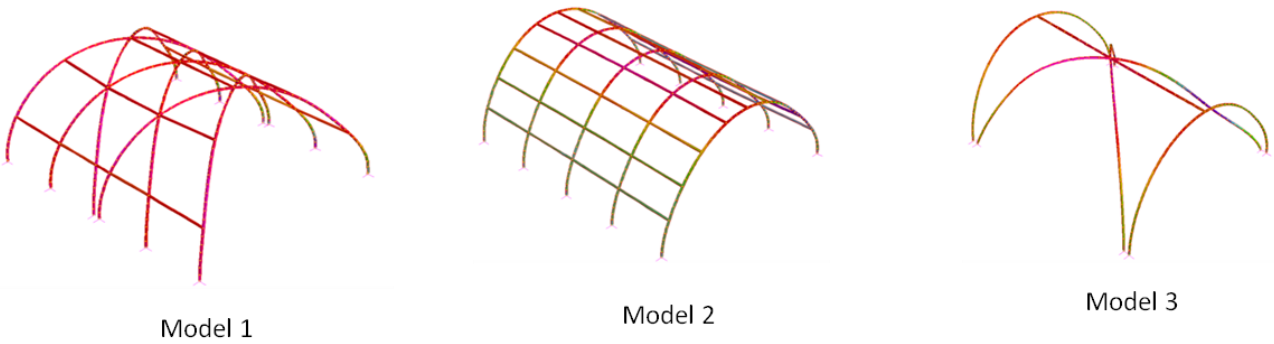


Figure 12. Displacement of models under serviceability limiting state (SLS): G + 0.7 Q + W (5% exaggeration).

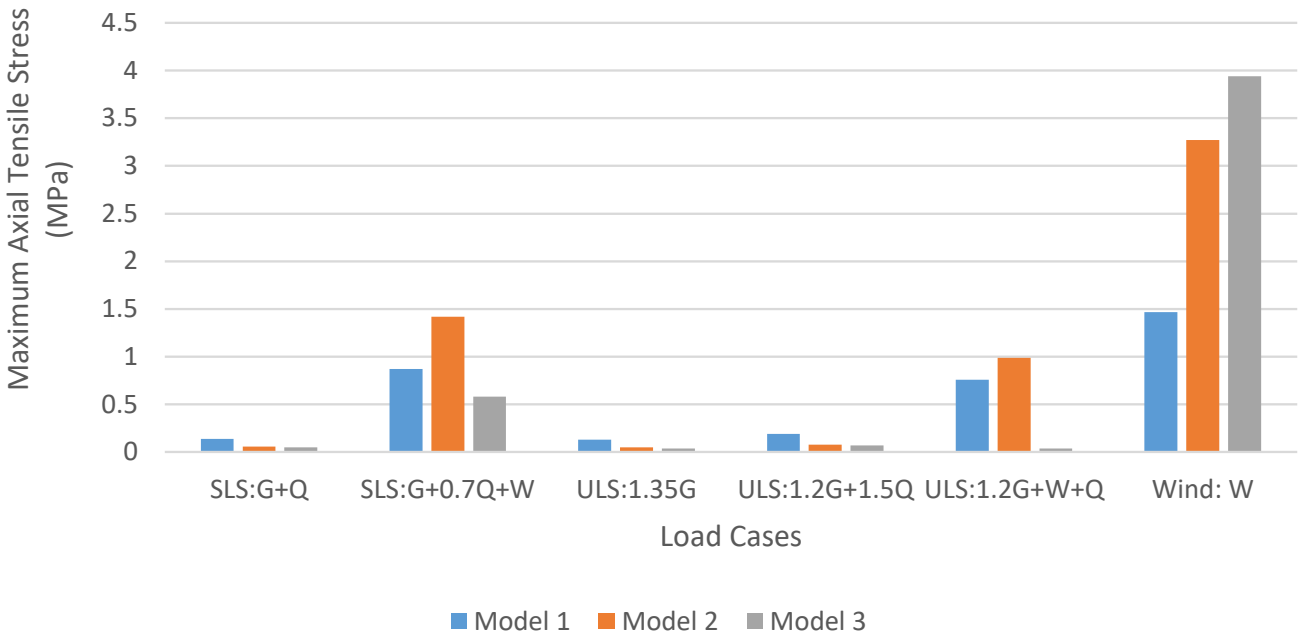


Figure 13. Maximum tension stress for varying load cases and models.

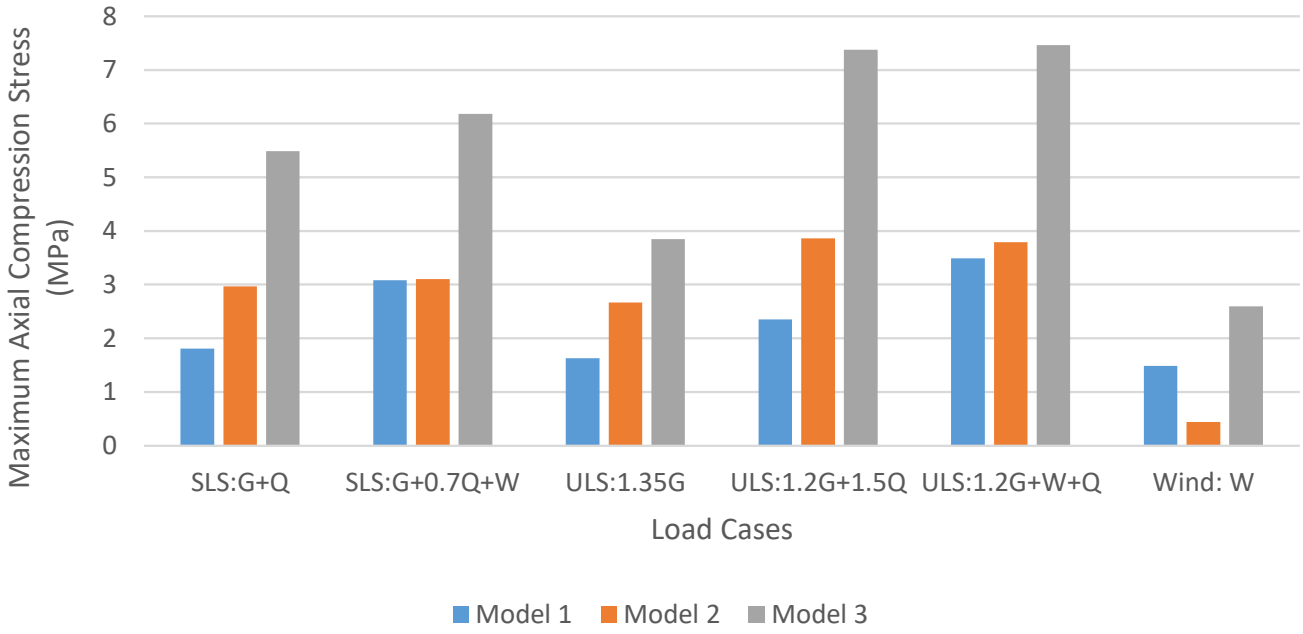


Figure 14. Maximum compression stress for varying load cases and models.

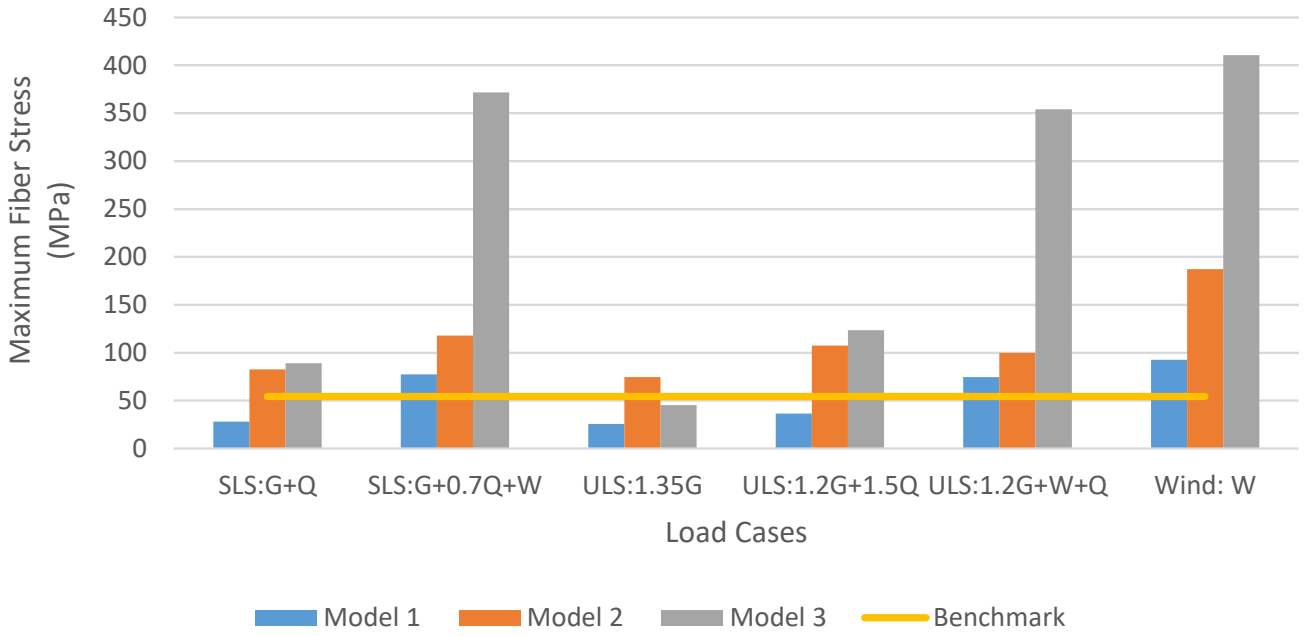


Figure 15. Maximum magnitude in fiber stress results in compression for varying load cases and models.

3.2.1. Displacement

The displacement measures the movement of structures from the original position. These results are summarized in Figure 11, as shown below. In Figure 11, the wind is shown giving the most deflection, but it can be countered by the dead and live load. Design 1 (model 1, similar for all models) can be seen behaving well at resisting dead and live loads but slightly worse for winds. Besides, design 2 performed equally for all loading cases but with the maximum dead load as a result of its heavy structure. In contrast, design 3 received a limited dead load because of its light structure but with varying deflection and the minimum deflection for dead and live load. However, design 3 had the maximum deflection for wind load. Figure 12 presents the deformation of the simulated frames due to the effect of the different combined actions.

3.2.2. Axial Stress

The axial stress measures the internal force of structures that results from axial forces. The axial stress, including tensile stress and compressive stress, was suggested by Strand7. These results are summarized graphically in Figures 12 and 13 for the tension and compression stresses, respectively. As shown in Figure 13, the tension stress for all designs mostly resulted from the wind load and only a slightly from the dead and live loads. This may be a result of the fact that both dead and live loads were acting downwards, hence, they only had a noticeable effect on the base. In addition, the tensile stress for all of the three models is the greatest in the SLS, including winds. It was found that for these downward cases, design 1 had the relatively largest tensile stress. This is mainly because of the cross-arches structure for distributing loads among the system, which causes more thrusts; hence, the restraints at the base are essential. Thus, the magnitude of tensile stress can be maximized because of combinations with wind loads. However, the magnitude was identified as low enough, which would not be greater than 296 MPa as the selected structure elements capacity.

Figure 14 shows that most of the compressive stresses come from the dead load and live load, with only little increases due to winds. Under wind loading, designs 1 and 2 had similar maximum compressive stress on the windward face, but design 1 had lower stress when there was no wind load. Design 3 had the most compressive stress for all cases,

without exceeding the capacity for bamboo scrimber (134.9 MPa). Comparing the graphs for tensile and compressive stresses, the compression was larger than the tension overall.

3.2.3. Total Fiber Stress

The stresses were determined based on the beams' cross-sections, so they were considered as the total fiber stress. They were computed based on the bending moments in two states of planes and axial directions. As fiber stress varies in different positions inside structural members, these results were summarized in terms of their maximum magnitude and are presented in Figure 14.

Figure 15 indicates that the fiber stress for model 3 was significantly higher because of wind, and the large deflection of model 3 represents the significance even more clearly. As shown in the figure, there was a 54.3 MPa limiting capacity of bamboo scrimber. Except for downward cases of G+Q and 1.35 G for model 1, all the other cases of the three models exceeded their limit and resulted in uneven load distribution throughout the members, which could further lead to serious failures of the whole structure. Hence, a new structure needs to be developed to address the issues.

3.2.4. Bending Stress

Figure 16 shows the results of the analysis for maximum magnitudes of bending stresses for different case combinations. The bending stress is determined in two different planes, including the beam element and the one that is perpendicular to it.

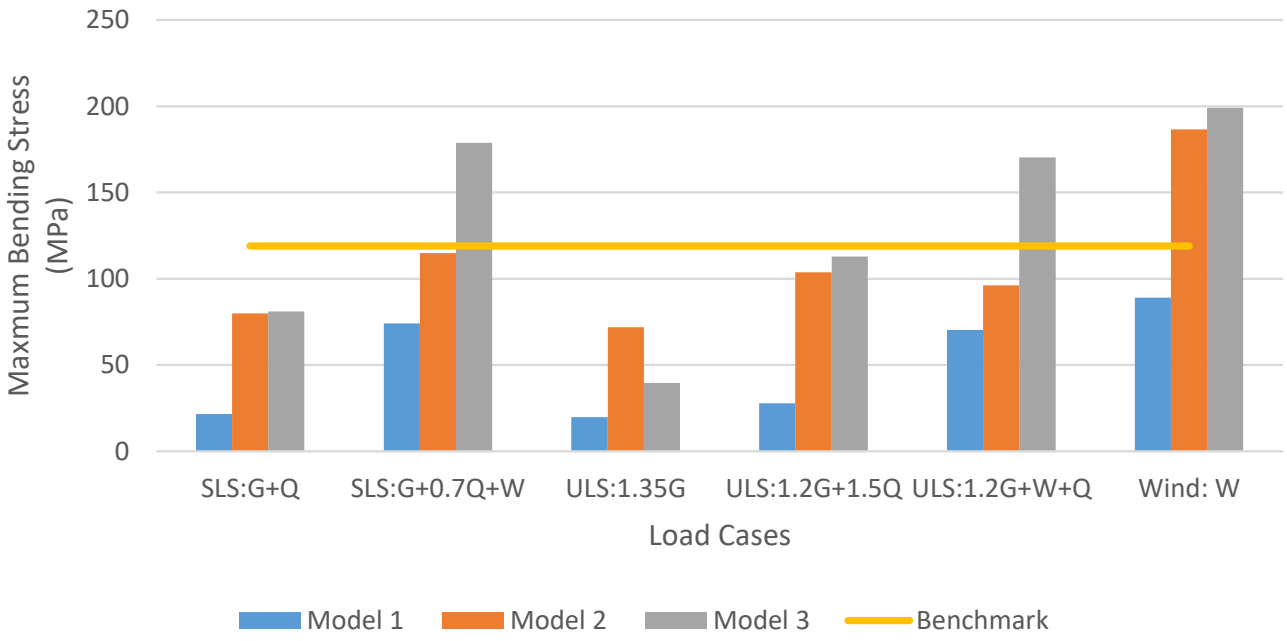


Figure 16. Maximum bending stress results for varying load cases and models on plane 1.

Figure 16 indicates that model 3 will fail under some SLS and ULS limiting states, as the stresses exceeded the capacity (a benchmark in Figure 15). As a result, the member with the stress higher than the capacity will fail. Consequently, the whole structure may collapse. Alternatively, stress is distributed evenly throughout the structure of designs 2 and 3. Therefore, the failure in bamboo scrimber can be avoided.

3.3. Static Load Analysis of the Proposed New Design

Three ultimate limiting load conditions and two serviceability limiting load conditions were considered for the new design. All the results are with the same geometry properties

as previously stated. Since the main objective needs to address the performance under wind loads, the wind load case is also presented in the following contents.

3.3.1. Axial Stress

Figure 17 shows two different types of axial stress covering both states of being in tension and in compression.

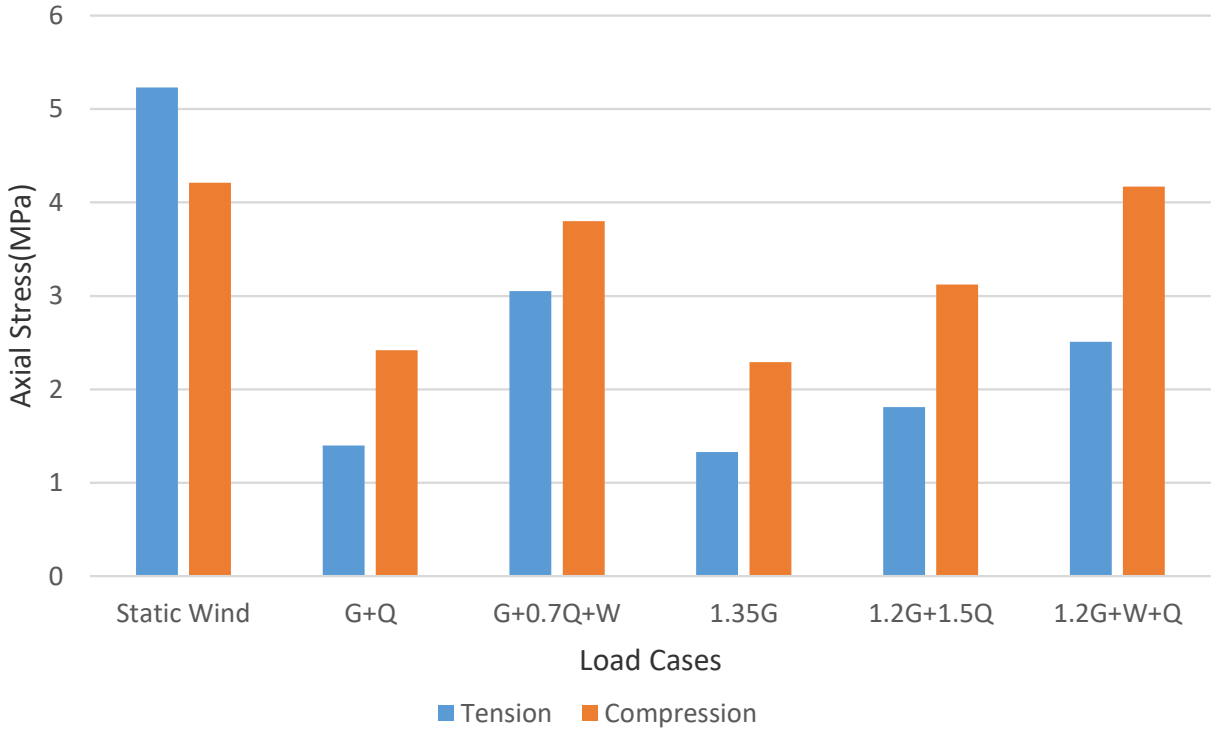


Figure 17. Summary of the maximum of two types of axial stress for different load cases of the proposed new design.

It becomes clear that both of the critical values for tension and compression occur at the static wind load case. It is noteworthy that tensile stress is greater than compressive stress under the static wind load case if compared with other cases. This is because wind load is a lateral load, which results in more tensile stresses; this also explained how the load cases involving wind load tended to have greater tension than those cases that did not consider wind load. From the previous table, which suggests an ultimate tensile stress of 296.2 MPa and an ultimate compressive stress of 134.9 MPa, the critical values of the proposed new design are much smaller than the ultimate values. It can be concluded that the performance of the new design under axial load conditions is governed.

3.3.2. Total Fiber Stress

Like axial stress, the total fiber stress of the structure can be either compression or tension due to the effects of the applied loads and the function of the structure system. Both types of stress are demonstrated in the figure below (Figure 18).

The figure suggests that the critical case was still the static wind load case for both tension and compression conditions. It is worth noting that tensile stress exceeded the compressive stress for the cases with wind loads compared with the cases under axial stress. Consequently, it is recommended that one should pay more attention to the performance of fiber under tensile stress when considering the wind load impacts. As can be seen from the figure, the critical fiber stress under the static wind load case is still smaller than the ultimate condition, hence, the proposed new solution is still under control in this case.

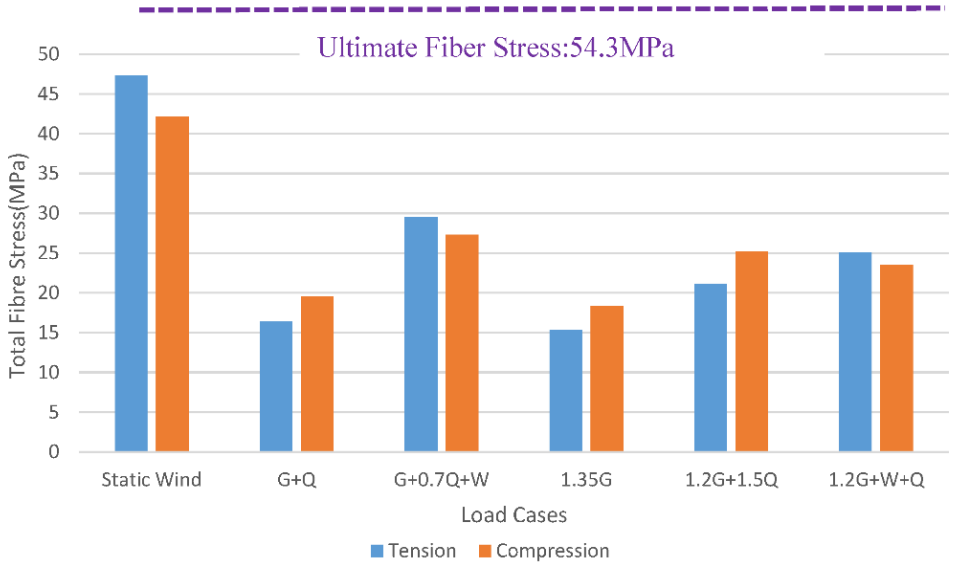


Figure 18. Summary of the maximum of two types of total fiber stress for different load cases of the proposed new design.

3.3.3. Bending Stress

The bending stress was conducted along two planes in Strand7. During the data collection process, it was found that, for all the load cases, the maximum condition occurred at plane 1 only. Therefore, only the bending in plane 1 was collected and summarized in the below figure (Figure 19).

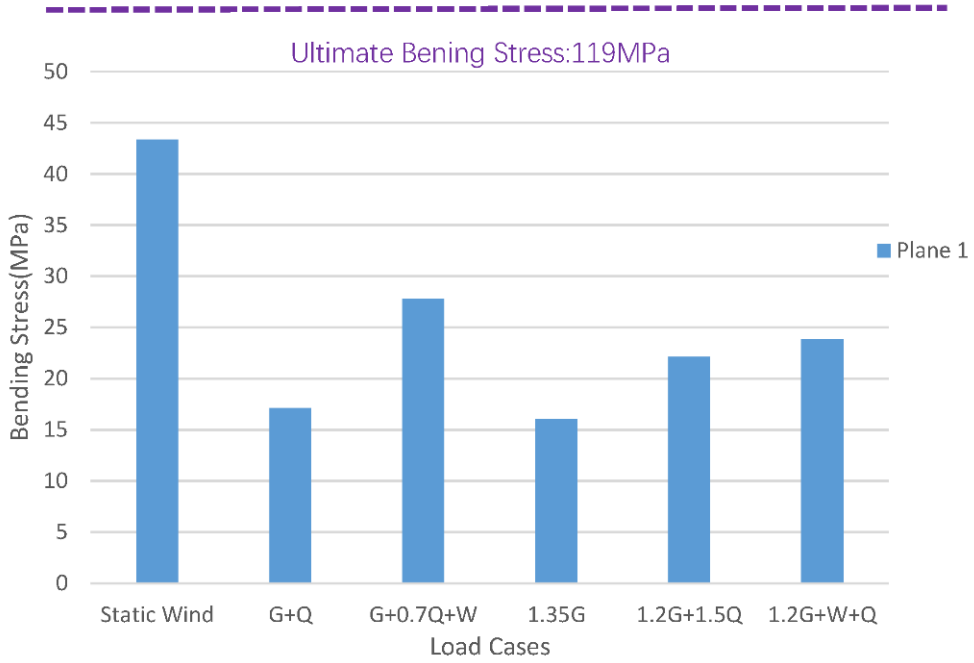


Figure 19. Summary of maximum bending stress for different load cases of the new design.

As can be seen from the figure, the maximum load still occurred under the static wind load case. The critical value was still significantly under the ultimate bending stress, and thus, the new design was safe under bending stress.

3.3.4. Summary of Static Load Analysis

In summary, under static load analysis, for all four designs, the critical case occurred under the static wind load case. Among the three initial designs, design 1 with a cross-arches structure had the best performance. Nonetheless, the structure of design 1 was still not feasible using bamboo scrimber under the fiber stress test.

A new design was proposed to overcome the demonstrated failure. Notwithstanding that the axial stress of the new design was bigger than the three initial designs, which was mainly due to the added complex structures, in no case did the axial stress values of the new design exceed the maximum bamboo scrimber capacity. Furthermore, the performance of the new design prevented potential failure from total fiber stress and demonstrated better bending stress resistance than initial design 1. Hence, it can be proved that the proposed new curved roof was feasible under static load conditions.

3.4. Dynamic Wind Load Analysis

3.4.1. Wind Speed Calculations

Assumptions

The location of the structure was Sydney, and the terrain category was taken to be terrain category 2. Since Sydney is in region A2, as outlined in the AS1170.2 [22] and assuming an average recurrence interval of 500 years, $V_R = 45$ ms^{-1} as shown in Table 3 of AS1170.2 [22]. Therefore, the terrain multiplier, taken from Table 4 of AS1170.2, for a height of 3 m, was terrain/height multiplier $M_{z,cat} = 0.91$ [6] (pp. 19–20). The shielding multiplier, $M_s = 1.0$, was taken from Table 4 of AS1170.2 as the most conservative case [6] (p. 21). For a better analysis, the heights of buildings in the surrounding area needed to be recorded and, utilizing clause 4.3 [22], a detailed analysis should return a more accurate shielding multiplier value. However, given the lack of a specific location for the structure, the most conservative case was taken. The topographic multiplier, $M_t = 1.0$, was taken from Section 3.4, and lee regions were ignored as per clause 4.4.3 as no lee zones are in Australia. This was not the most conservative case, as $M_h > 1.0$ and $M_t > 1.0$. However, because of a lack of specified location, the analysis for the topography of the site could not be analyzed. This would have been done by utilizing geospatial software to model the topography around the site and by conducting an analysis on the maximum height of hills in that region.

Calculating Wind Speed

Since M_d was the most conservative case, $v_{des,\theta} = 45 \times 1.0 \times 0.91 \times 1.0 \times 1.0 = 40.95$ ms^{-1}. It should be noted, however, that a static wind analysis using the values found in AS1170.2 [22] and utilized in previous years is not an accurate representation of wind effects on a structure over a long period of time. This is because the values utilized refer to the gust wind speed, which is a maximum wind speed event with a duration outlined in AS1170.2 [22] as being a 0.2-s gust event. This means that structures will be over-designed to resist this maximal value for wind speeds that are unlikely to occur. This is because the wind recordings in Table 3 are based on historical records where the maximum wind speed is taken without distinguishing whether it is from a synoptic wind or a thunderstorm event. These two wind events have different profiles and, for a smaller structure, since the standard just records the maximum event, there is the possibility that the wind speed is based on a thunderstorm event. Hence, if this was used to define the normal response to a structure for winds occurring regularly, then there would have been the potential for overdesigning of the structure. Instead, it would be more advantageous to analyze a structure's response to a larger duration wind event.

Since a synoptic wind event is made up of two parts; a mean component and a fluctuating component, the fluctuating component is responsible for the dynamic effects induced by wind loads, and for roof structures on which the wind speeds have the most effect, due to the increasing wind speed as elevation increases, the roof is going to have the most adverse effects due to wind loading.

Using the equation,

$$v_{gust} = G\overline{v}, \tag{3}$$

where:

v_{gust} = the gust wind speed

$$G = \left(1 + g\left(\frac{\sigma}{\overline{v}}\right)\right) \tag{4}$$

$\frac{\sigma}{\overline{v}}$ = turbulence Intensity, I_z

Turbulence intensity is found in Table 6 of AS1170.2 [22] and is a measure of the turbulence in the wind. Wind turbulences are responsible for a phenomenon known as turbulence buffeting, where the turbulence induces a dynamic response in the structure. This can occur both in the along-with-wind and the crosswind direction—Table 7 summarizes different extracted dynamic modes in different models.

$$g = \sqrt{1.2 + 2\log_e(Tn_a)} \tag{5}$$

Table 7. Natural frequencies under different modes for the four models.

	N_a (1st Mode)	N_a (2nd Mode)	N_a (3rd Mode)	N_a (4th Mode)
Model 1	6.08772	11.9478	12.9541	14.1401
Model 2	6.08232	8.37319	8.63187	13.0552
Model 3	6.37322	7.11168	8.90585	9.72662
New Model	5.91085	11.7663	11.8231	13.4578

This assumed that the peak factor is based on the hourly mean wind speed, hence, the period was 1 h, or 3600 s, where:

n_a, the natural frequency of the first mode

Using the value of the peak factor in the gust factor equation and rearranging the gust wind speed equation gives: $\overline{v} = \frac{v_{gust}}{G}$.

The values for the calculation are summarized in Table 8:

Table 8. Calculation of wind speed of the four models.

	Natural Frequency of First Mode, n_a (Hz)	Peak Factor	Gust Factor	Mean Wind Speed, $\overline{v}$ (ms^{-1})
Model 1	6.088	4.603	1.902	21.527
Model 2	6.082	4.603	1.902	21.528
Model 3	6.373	4.613	1.904	21.505
New Design	2.931	4.442	1.871	21.892

Using Davenport's equation for the power spectrum distribution:

$$s_u(n) = 4k\overline{v}^2 \frac{x^2}{n(1+x^2)^{\frac{4}{3}}} \tag{6}$$

where $x = \frac{1200n}{\overline{v}}$

n is the frequency (Hz)

$\overline{v}$, mean wind velocity (ms^{-1})

k is surface roughness (taken as 0.05 for terrain category 2)

Rearranging the Davenport equation where the pressure spectrum distribution (PSD) value is dependent on the frequency gives:

$$s_u(n) = 4k\frac{(1200)^2 n}{\left(1+\left(\frac{1200n}{\overline{v}}\right)^2\right)^{\frac{4}{3}}} \tag{7}$$

This is the spectrum for the wind speed. Utilizing the fact that the velocity component for wind speed is based on a mean and fluctuating component provides:

$$\text{Fluctuating wind velocity, } v(t) = \overline{v} + v'(t)$$

where $v'(t)$ is the fluctuating component of the velocity.

Using the fact that the drag force, $F_D = \frac{C_d\rho}{2}A(v(t))^2$ where:

The drag coefficient, C_d = 1.2 (semi-cylindrical roof shape)
Density of the air, ρ_{air} = 1.2 kg/m^3
The projected area, A

By squaring the value of the wind velocity, $(v(t))^2 = \overline{v}^2 + 2\overline{v}v'(t) + (v'(t))^2$.
Since the value for $(v'(t)) \approx 0$

$$F_D = \frac{C_d\rho}{2}A(v(t))^2 = \frac{C_d\rho}{2}A\left(\overline{v}^2 + 2\overline{v}v'(t)\right)^2$$

$$\frac{C_d\rho}{2}A\left(\overline{v}^2 + 2\overline{v}v'(t)\right) = \frac{C_d\rho}{2}A\overline{v}^2 + C_d\rho A2\overline{v}v'(t) \tag{8}$$

The wind force due to the mean wind speed is $\frac{C_d\rho}{2}A\overline{v}^2$ and the fluctuating component is $C_d\rho A\overline{v}v'(t)$ [7] (p. 2).

Since the fluctuating component is responsible for the dynamic effects on the building:

$$S_f(n) = \frac{(F'_D(t))^2}{Hz} = \frac{C_d^2\rho^2A^2\overline{v}^2(v'(t))^2}{Hz} \tag{9}$$

Since the fluctuating velocity spectrum can be written as, $S_u(n) = \frac{(v'(t))^2}{Hz}$.
Therefore, the equation for $S_f(n) = C_d^2\rho^2A^2\overline{v}^2S_u(n)$:

$$S_f(n) = C_d^2\rho^2A^2\overline{v}^2\ 4k\frac{(1200)^2 n}{\left(1+\left(\frac{1200n}{\overline{v}}\right)^2\right)^{\frac{4}{3}}} \tag{10}$$

Dividing the force spectrum by the square of the area, A, will result in the pressure spectrum:

$$S_p(n) = C_d^2\rho^2\overline{v}^2\ 4k\frac{(1200)^2 n}{\left(1+\left(\frac{1200n}{\overline{v}}\right)^2\right)^{\frac{4}{3}}} \tag{11}$$

Since each of the models have different values, the pressure spectrum for each model are shown below.

Pressure spectrum for model 1:

$$S_p(n) = 1.2^2 \times 1.2^2 \times 21.527^2 \times 4 \times 0.05 \times \frac{(1200)^2 n}{\left(1 + \left(\frac{1200}{21.527}\right)^2\right)^{\frac{4}{3}}} \quad (12)$$

Pressure spectrum for model 2:

$$S_p(n) = 1.2^2 \times 1.2^2 \times 21.528^2 \times 4 \times 0.05 \times \frac{(1200)^2 n}{\left(1 + \left(\frac{1200}{21.528}\right)^2\right)^{\frac{4}{3}}} \quad (13)$$

Pressure spectrum for model 3:

$$S_p(n) = 1.2^2 \times 1.2^2 \times 21.505^2 \times 4 \times 0.05 \times \frac{(1200)^2 n}{\left(1 + \left(\frac{1200}{21.505}\right)^2\right)^{\frac{4}{3}}} \quad (14)$$

Pressure spectrum for the new model:

$$S_p(n) = 1.2^2 \times 1.2^2 \times 21.892^2 \times 4 \times 0.05 \times \frac{(1200)^2 n}{\left(1 + \left(\frac{1200}{21.892}\right)^2\right)^{\frac{4}{3}}} \quad (15)$$

Tables 9–12 show the classification of the main dynamic structural responses that can be extracted in different simulated models. The presented structural reactions were varied from the maximum displacement in different directions as well as the critical stresses. The presented technical values can help to provide a proper procedure in the hands of the practical engineers when it comes to designing of the light structures to meet both serviceability and ultimate requirements.

Table 9. Maximal displacements in roof members using bamboo scrimber based on Davenport's wind spectrum.

Scrimber	DX (mm)	DY (mm)	DZ (mm)
Model 1	1.72	77.96	169.50
Model 2	0.16	58.62	113.20
Model 3	42.65	123.80	193.50
New Model	0.46	3.45	8.42

Table 10. Maximal displacements in roof members using natural bamboo based on Davenport's wind spectrum.

Natural Bamboo	DX (mm)	DY (mm)	DZ (mm)
Model 1	0.71	32.13	69.95
Model 2	0.07	24.32	47.00
Model 3	17.55	51.02	79.86
New Model	0.87	1.68	4.09

Table 11. Maximal stresses in the roof members using bamboo scrimber based on Davenport's wind spectrum.

	σ_{axial} (MPa)	σ_{bend} (MPa)	σ_{fibre} (MPa)	σ_{shear} (MPa)	$\sigma_{shear,avg}$ (MPa)
Model 1	0.37	67.77	69.09	0.62	0.41
Model 2	0.29	55.06	55.12	0.52	0.35
Model 3	0.39	65.22	97.52	0.53	0.35
New Model	0.91	17.52	18.33	0.39	0.26

Table 12. Maximal stresses in the roof members using natural bamboo based on Davenport's wind spectrum.

	σ_{fibre} (MPa)	σ_{axial} (MPa)	σ_{bend} (MPa)	σ_{shear} (MPa)	$\sigma_{shear,avg}$ (MPa)
Model 1	28.75	0.26	28.59	0.56	0.29
Model 2	23.35	0.21	23.31	0.47	0.25
Model 3	30.72	0.28	27.55	0.48	0.25
New Model	8.56	0.69	8.12	0.36	0.19

Figure 20 presents a possible model of the failure shape of model 2 due to the effect of the applied dynamic wind loading. As illustrated, a combination of bending and twisting can be found as the main failure modes in the simulated structures. The extracted modes are significantly important when it comes to designing suggested frames because of the effect of the dynamic wind loading. Additionally, the suggested concept might be extended into calculating and predicting the structural responses due to the influence of the buckling and post-buckling analysis of the simulated frames.

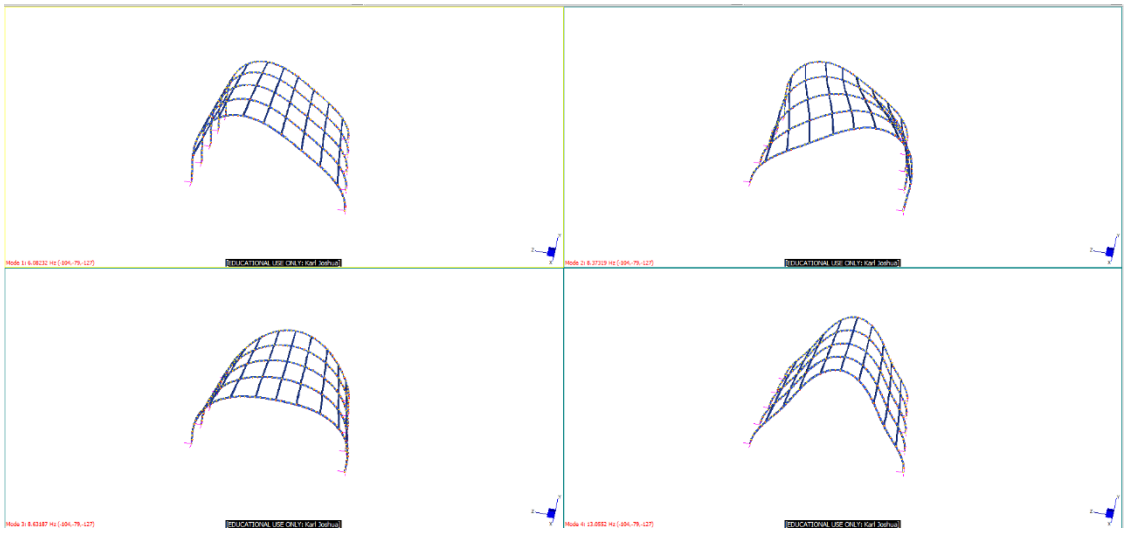


Figure 20. Frame representation due to the effect of the dynamic wind loading in model 2 vibration.

The same approach is presented in Figure 21. Based on the simulated effect of the dynamic wind loading, which was applied to frame model 3, a combination of the shear and twisting failure modes are presented in Figure 21. The obtained failure modes were fully dependent on the suggested shape of the frames.

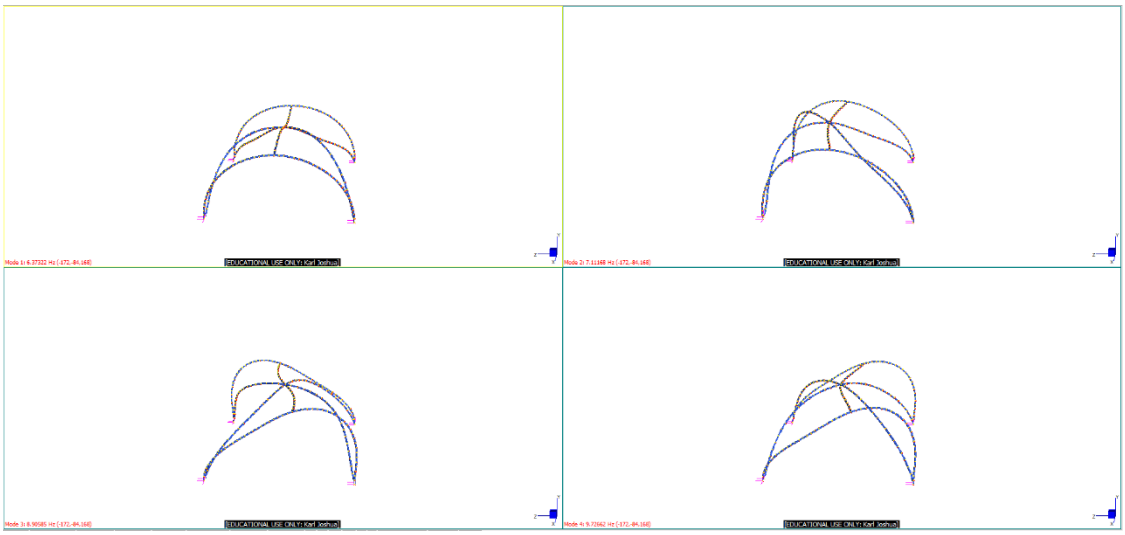


Figure 21. Frame representation due to the effect of the dynamic wind loading in model 2 vibration.

3.5. Discussion of Dynamic Wind Load

Assumptions were made in the calculation of the spectral load. For the pressure spectrum distribution, it was assumed that a unit pressure would be applied to the windward face of the structure; however, as can be seen from the spectral analysis, replacing bamboo with the engineered bamboo (scrimber) had an adverse effect on the resistance to dynamic loading. This is most likely due to the improper selection of the geometry. It should be noted that the factors for the spectrum wind load (Davenport's equation) had load factors that were higher in frequencies less than 1 Hz. Since the natural frequencies of all the structures were of greater magnitude than 1 Hz, this meant that resonance would not have as adverse an effect on the structure. This would change, however, if the roof was situated on a high-rise structure. This is because the natural frequency of the structure would go down and the frequency of the fluctuations in the wind would be closer to the natural frequency of the structure, resulting in resonance relating to large displacements in the structure. However, since the spectral analysis was based on the structure at the height of 3 m it is unlikely that the effects of dynamic wind loading would be significant. Whilst the dynamic loads are not inherently covered by past projects, it is an integral component of understanding the wind's effect on structures, especially when it relates to structural dynamics. This is because dynamic movement induces fatigue effects in materials, with bamboo also being affected. Whilst bamboo, where the loads run parallel to the culm axis, will not result in failure induced by fatigue, fatigue failure does occur when the load is acting perpendicular to the culm axis. This is related to the anisotropic nature of bamboo perpendicular to the culm axis, where the load-carrying capacity of the member is significantly reduced. This is important because dynamics in a structure are formed as a result of cyclic loads, and fatigue effects can result in the fatigue failure of a structure well below its capacity. Therefore, from a design perspective, structural dynamics are incredibly important. The maximum result for the spectral wind response was taken from the spectral load case SRSS (Spectral Response extracted from the spectral load case), in which the maximum response of the building due to the spectrum load was recorded. These are seen in the presented tables. This is done because 25 different modes of vibration were analyzed, each with their own specific natural frequency; however, because most of the energy was contained within the first few modes of vibration, the other modes were done for a more robust analysis. As can be seen from the new model, there was a decrease in the total fiber stress observed in the revised new model (Figure 22).

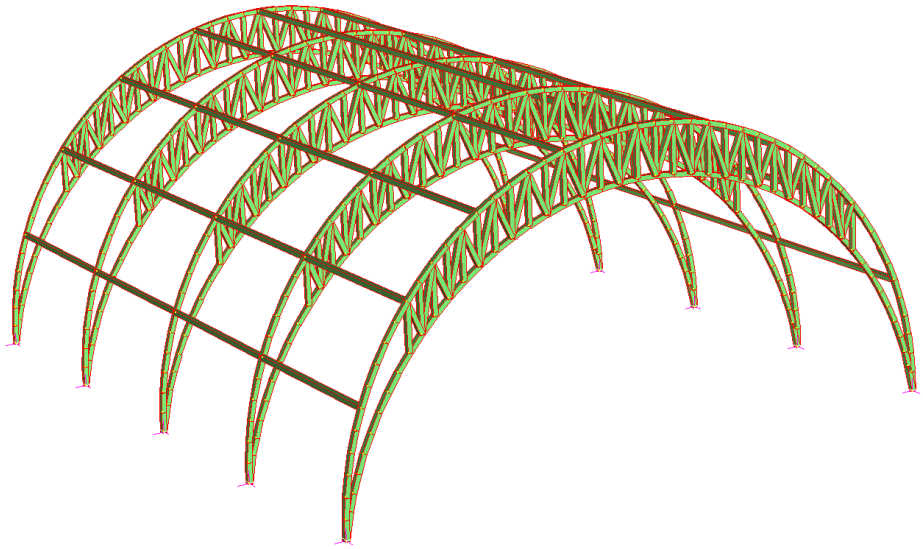


Figure 22. Desirable bamboo structural design solution.

This was mainly due to the increased load paths created by the pseudo truss that acted as bracing for wind in the lateral direction. There were more load paths for the wind load to go through, hence, the stresses in the material were not as large as observed from the results. In contrast, for the case of the bamboo scrimber, increased loading was observed when the dynamic analysis was done. This may have been due to the error in the selection of a cross geometry 0.45×0.45 rectangular section. Because of the flexibility of bamboo, it is a more useful structural element under dynamic loads, where the flexibility allows for greater vibrational energy to be dissipated because of the inherent flexibility of the member. The solid bamboo scrimber, because of its higher rigidity, is more affected by the wind energy through the fluctuations due to greater stiffness. Hence, this energy cannot be easily dissipated, and this results in higher forces in the sections.

4. Conclusions

This study proposed potential design solutions for implementing curved manufactured bamboo roof structures. Three initial designs were suggested to analyze their static load behavior and the corresponding dynamic wind load resistances using finite element analysis through Strand7. It was found that design 1 with a cross-arches structure is the most functional design solution among the three under static load analysis. However, it still failed the fiber stress test, which could lead to potential fracture of the structure. Hence, a new roof was proposed to address the issue, as shown in the figure below. With the new solution, which consists of lower arches and a truss system, the structure can withstand the fiber stress and bring a better performance on bending stress toughness under static wind load. Further analyzing the four designs under the dynamic wind load case, it was found that the proposed new design had the best function among all the models. Natural bamboo material, in contrast, performed better than bamboo scrimber for the new design. After conducting the buckling analysis, it was found that bamboo scrimber tends to undergo buckling more easily than natural bamboo, which may be because of its shape and the relatively high stiffness.

One potential improvement of the proposed design is to change the shape of bamboo scrimber. This can be done by increasing the height of the scrimber to increase the stress capacity or by changing the shape from a rectangular to an I-shape. However, the latter solution is hard to achieve in reality because of the property of bamboo. Nonetheless, the new proposed structure is still desirable because of its extraordinary performance under various load types. If one considers further improvements to the performance of the new design under dynamic loads and buckling, alternative bamboo material with better shapes should be taken into account. This study focused on designing and optimizing

the particular type of structures considering the structural and architectural engineering research. The main novelty of the current study was to suggest a simple and reliable finite element method to design some unique structures for which there are no practical guidelines in practice.

Author Contributions: Conceptualization: all authors; literature review, research method: all authors; software: Y.M., K.J., Y.Y., and J.L.; drafting the article based on the numerical reports: F.T. and S.S.; resources and interpretation: F.A.M. and F.T. All authors have read and agreed to the published version of the manuscript.

Funding: This research received no external funding.

Institutional Review Board Statement: Not applicable.

Informed Consent Statement: Not applicable.

Data Availability Statement: Not applicable.

Acknowledgments: The authors would like to express their deepest appreciation to the University of New South Wales and the University of Sydney for providing convenient places and resources to undertake the current research.

Conflicts of Interest: The authors declare no conflict of interest.

References

1. Habibi, S. Design concepts for the integration of bamboo in contemporary vernacular architecture. *Archit. Eng. Des. Manag.* **2019**, *15*, 475–489.
2. De Flander, K. The Role of Bamboo in Global Modernity: From Traditional to Innovative Construction Material. Ph.D. Thesis, Wageningen University, Wageningen, The Netherlands, 2005.
3. Maikol, S.M.Y.; Maksimovich, S.V.; Ivanovna, B.G.; Ainur, S. Bamboo Structures for Modern Sustainable Architecture. *ISVS e-J.* **2020**, *7*, 27–39.
4. Yu, Y.L.; Zhu, R.; Wu, B.; Hu, Y. Fabrication, material properties, and application of bamboo scrimber. *Wood Sci. Technol.* **2015**, *49*, 83–98. [CrossRef]
5. Strand7 Computer Software (Version 2.4.6). Available online: https://www.strand7.com/ (accessed on 20 February 2021).
6. Wei, Y.; Ji, X.; Duan, M.; Li, G. Flexural performance of bamboo scrimber beams strengthened with fiber-reinforced polymer. *Constr. Build. Mater.* **2017**, *142*, 66–82. [CrossRef]
7. Escamilla, E.Z.; Habert, G. Environmental impacts of bamboo-based construction materials representing global production diversity. *J. Clean. Prod.* **2014**, *69*, 117–127. [CrossRef]
8. Sharma, B.; Gatóo, A.; Ramage, M.H. Effect of processing methods on the mechanical properties of engineered bamboo. *Constr. Build. Mater.* **2015**, *83*, 95–101. [CrossRef]
9. Escamilla, E.Z.; Habert, G.; Daza, J.F.C.; Archilla, H.F.; Fernández, J.S.E.; Trujillo, D. Industrial or traditional bamboo construction? Comparative life cycle assessment (LCA) of bamboo-based buildings. *Sustainability* **2018**, *10*, 3096. [CrossRef]
10. Sharma, B.; van der Vegte, A. Engineered bamboo for structural applications. In *Nonconventional and Vernacular Construction Materials*; Elsevier: Amsterdam, The Netherlands, 2020; pp. 597–623.
11. Chen, M.; Ye, L.; Li, H.; Wang, G.; Chen, Q.; Fang, C.; Dai, C.; Fei, B. Flexural strength and ductility of moso bamboo. *Constr. Build. Mater.* **2020**, *246*, 118418. [CrossRef]
12. Correal, F.F. Bamboo design and construction. In *Nonconventional and Vernacular Construction Materials*; Elsevier: Amsterdam, The Netherlands, 2020; pp. 521–559.
13. Lorenzo, R.; Mimendi, L.; Godina, M.; Li, H. Digital analysis of the geometric variability of Guadua, Moso and Oldhamii bamboo. *Constr. Build. Mater.* **2020**, *236*, 117535. [CrossRef]
14. Sun, X.; He, M.; Li, Z. Novel engineered wood and bamboo composites for structural applications: State-of-art of manufacturing technology and mechanical performance evaluation. *Constr. Build. Mater.* **2020**, *249*, 118751. [CrossRef]
15. Lin, Q.; Huang, Y.; Li, X.; Yu, W. Effects of shape, location and quantity of the joint on bending properties of laminated bamboo lumber. *Constr. Build. Mater.* **2020**, *230*, 117023. [CrossRef]
16. Sharma, B.; Gatóo, A.; Bock, M.; Mulligan, H.; Ramage, M. Engineered bamboo: State of the art. *Proc. Inst. Civ. Eng. Constr. Mater.* **2015**, *168*, 57–67. [CrossRef]
17. Putri, A.H.; Dewi, O.C. Overview of Bamboo Preservation Methods for Construction Use in Hot Humid Climate. *Int. J. Built. Environ. Sci. Res.* **2020**, *4*, 1–10.
18. Vogtländer, J.; Van der Lugt, P.; Brezet, H. The sustainability of bamboo products for local and Western European applications. LCAs and land-use. *J. Clean. Prod.* **2010**, *18*, 1260–1269. [CrossRef]

19. Bonilla, S.H.; Guarnetti, R.L.; Almeida, C.; Giannetti, B. Sustainability assessment of a giant bamboo plantation in Brazil: Exploring the influence of labour, time and space. *J. Clean. Prod.* **2010**, *18*, 83–91. [CrossRef]
20. Dai, Y.; Hwang, S.-H. Technique, creativity, and sustainability of bamboo craft courses: Teaching educational practices for sustainable development. *Sustainability* **2019**, *11*, 2487. [CrossRef]
21. Trujillo, E.; Moesen, M.; Osorio, L.; Van Vuure, A.W.; Ivens, J.; Verpoest, I. Bamboo fibres for reinforcement in composite materials: Strength Weibull analysis. *Compos. Part A Appl. Sci. Manuf.* **2014**, *61*, 115–125. [CrossRef]
22. Pham, L. Actions on Structures: Regulations and Standards. Available online: https://wenku.baidu.com/view/33714931f705cc175427096b.html (accessed on 20 February 2021).
23. Sivanerupan, S.; Wilson, J.L.; Gad Swinburne, E. Structural analysis and design of glazed curtain wall systems. *Aust. J. Struct. Eng.* **2011**, *12*, 57–67.
24. Buttenshaw, S.; Mullard, J. Dynamic Analysis of Mine Blasting using the Spectral Response Analysis Methods of AS1170.4. In Proceedings of the Australian Earthquake Engineering Society 2019 Conference, Newcastle, UK, 29 November–1 December 2019.
25. Standard, B. Eurocode 1: Actions on Structures. Available online: http://www.hwa.uk.com/site/wp-content/uploads/2018/02/CD.POL_.24B-BS-EN-1991-Part-1-1-20021.pdf (accessed on 20 February 2021).
26. Cook, N. *Designers' Guide to EN 1991-1-4 Eurocode 1: Actions on Structures, General Actions Part 1–4. Wind Actions*; Thomas Telford Publishing: London, UK, 2007.
27. Blackmore, P.; Tsokri, E. Wind loads on curved roofs. *J. Wind Eng. Ind. Aerodyn.* **2006**, *94*, 833–844. [CrossRef]